Journal of Information Hiding and Multimedia Signal Processing ©2016 ISSN 2073-4212
Ubiquitous International Volume **7**, Number **3**, May **2016**

An Image Splicing Detection Method Based on PCA Minimum Eigenvalues

Lifei Zhan, Yuesheng Zhu and Zhiwei Mo

Communication and Information Security Lab
Institute of Big Data Technologies, Shenzhen Graduate School
Peking University, China
zhanlf@sz.pku.edu.cn; zhuys@pku.edu.cn; mozhiwei@sz.pku.edu.cn

Received September, 2015; revised February, 2016

Abstract. *This paper presents a novel and effective image splicing forgery detection method based on the inconsistency of irrelevant components between the original and the tampered regions. The specific irrelevant components can be described by the minimum eigenvalues obtained by the principal component analysis (PCA) without knowing any prior information. To avoid the impact of local structures, a pixel and its nearest neighbors are taken as a block and the input matrix of PCA are gotten through self similarity pixel strategy (SSS) from the block, which extracts a local minimum eigenvalue for every pixel. The experimental results on several forged image datasets demonstrate that our method achieves competitive detection accuracy compared with two other region-based methods.*
Keywords: Splicing forgery; Digital image forensics; Principal component analysis; Minimum eigenvalue; Self similarity pixel strategy.

1. **Introduction.** With the rapid development of multimedia and network technology, digital images, as an effective carrier of information, are having a more and more important impact on people's daily lives. However, the image content can easily be tampered with the increasingly powerful image processing software, which threatens the integrity and authenticity of digital images. Moreover, if the tampered images were used for illegal purposes, there would be no doubt causing extremely bad effects on both the individual and society. Therefore how to effectively detect the tampered images has an urgent and practical significance. In this paper, we will focus on image splicing forgery detection, which is a common image manipulation to distort an image by composing or merging two regions from different source images together.

In recent years, many image splicing detection methods are proposed, which can be classified into two categories: boundary based methods and region based methods [1]. The boundary based methods, just as the name implies, detect the splicing boundaries which are the salient parts [2] of an image by extracting the abnormal transient features to identify the forgery. Fang *et al.* [3] gave an example that utilized the sharp boundaries in color images. Similarly, high order spectral (HOS) [4], Hilbert-Huang transform (HHT) [5] and Wavelet analysis [6] were also used in image splicing forgery detection. Ng T.T. [7] further developed an edge-profile based method for extraction of CRF signature from a single image. Zhao *et al.* [8] proposed another method by using four gray level run-length run-number (RLRN) vectors along different directions obtained from de-correlated chroma channels as the input feature for SVM. Then Moghaddasi *et al.* [9] improved the

efficiency of RLRN detection algorithm by applying two dimension reduction methods, namely the PCA and kernel PCA. However, the boundary based methods need to satisfy some assumptions that splicing boundary doesn't suffer from blur or compression and usually cannot localize the tampered region.

The region based methods generally build on inconsistent features extracted from the splicing and the original regions to identify the forgery by dividing the image into local blocks or by image segmentation [10, 11]. Jan *et al.* [12] proposed a method based on detecting the presence of the camera pattern, which is under the assumption that the camera noise pattern is available in advance. Popescu *et al.* [13] established a bilinear model to describe the correlation caused by Color Filter Array (CFA) interpolation, and the Fisher classifier is employed for classification. Johnson *et al.* [14] proposed a model based on the lighting inconsistency by estimating the direction of light source for different objects or people in an image relying on some simply hypotheses. Nevertheless, these methods [12–14] require for certain prior knowledge while in most situations we are only given a suspicious image without any other information. In contrast to these approaches, blind noise estimation methods [15–17] work in the absence of the prior knowledge and achieve a better effect simultaneously, which detect the inconsistency of the background noise in splicing image.

In this work, taking the region irrelevant component into account, we propose a novel image splicing detection method based on PCA, through which we can easily get local minimum eigenvalues as a feature property of an image without knowing any prior information. More appealingly, it is affected little by edges, axis and brightness of image itself and can achieve high detection accuracy on pixel level.

The rest of this paper is organized as follows. In section 2, we introduce the PCA algorithm that will be used to calculate the minimum eigenvalues. Section 3 describes the concrete steps of our method. The experiment results and the analysis are minutely presented in Section 4. Finally, the paper is concluded in Section 5.

2. Principal Component Analysis (PCA).

2.1. Brief Summary of PCA.

PCA definition: for a given $m \times n$ matrix $X = [\mathbf{x}_1\ \mathbf{x}_2\ \cdots\ \mathbf{x}_n]$, where $x_i = [x_{1i}\ \ x_{2i}\ \ \cdots\ \ x_{mi}]^T (i = 1, 2, \cdots n)$ denotes a column of X, there is a linear transformation $R = [\mathbf{r}_1\ \mathbf{r}_2\ \cdots\ \mathbf{r}_n]^T$, where $r_i = [r_{i1}\ r_{i2}\ \cdots\ r_{in}]$, that

$$F = RX \tag{1}$$

$F = [\mathbf{f}_1\ \mathbf{f}_2\ \cdots\ \mathbf{f}_n]$, which satisfies three conditions: i. $\mathbf{r}_i \perp \mathbf{r}_j$, if $i \neq j$; ii. $Var(\mathbf{f}_1) \geq Var(\mathbf{f}_2) \geq \cdots \geq Var(\mathbf{f}_n)$; iii. $\parallel \mathbf{r}_i \parallel = 1 (i = 1, 2, \cdots m)$. Then $\mathbf{f}_i$ can be called the ith principal component [18].

It can be derived from the definition that the variance of F is

$$Var(F) = Var(RX) = diag(\lambda_1, \lambda_2, \cdots, \lambda_m) \tag{2}$$

Let Σ denote the covariance matrix of X

$$\Sigma = Cov(X) = \frac{1}{n-1}(X - \overline{X})(X - \overline{X})^T \tag{3}$$

and $\overline{X} = E[X] = \frac{1}{n}\sum_{i=1}^{n} \mathbf{x}_i$. There is an orthogonal matrix V

$$\Sigma = V^T \Lambda V, \Lambda = diag(\lambda_1, \lambda_2, \cdots, \lambda_m) \tag{4}$$

where λ_i is the ith eigenvalue of Σ in descending order, $\mathbf{v}_i$ is the eigenvector corresponding to eigenvalue λ_i. V meets the conditions of $R, i.e.$, $F = VX$ is a PCA expression of X.

2.2. **Image PCA Model.** Let matrix Y represent an observed image which includes the original image X and the Gaussian noise N_g . Assume that X can be decomposed into a low-rank component L whose rank is lower than $X's$ and a small perturbation component N_0 [19]. It can be given as

$$Y = X + N_g = L + N_0 + N_g \tag{5}$$

where L denotes the relevant component of an observed image and $N(N = N_0 + N_g)$ denotes the irrelevant component. Then

$$Cov(Y) = Cov(L + N) = E(LL^T) + E(NN^T) = Cov(L) + Cov(N) \tag{6}$$

Let $\Sigma_Y = Cov(Y),\ \Sigma_L = Cov(L),\ \Sigma_N = Cov(N)$ and the eigenvalue decomposition is

$$\Sigma_Y = V_Y^T \Lambda_Y V_Y = V_L^T \Lambda_L V_L + \Lambda_N = V_L^T (\Lambda_L + \Lambda_N) V_L \tag{7}$$

It can be inferred that

$$\Lambda_Y = \Lambda_L + \Lambda_N \tag{8}$$

And the PCA transformation matrix of L is the same as Y , *i.e.*, $V_Y = V_L$.

2.3. **Minimum Eigenvalue.** This paper focuses on the eigenvalues Λ_Y obtained from above. Let $\Lambda_Y = diag(\lambda_1, \lambda_2, \cdots, \lambda_m)$, $\Lambda_L = diag(\lambda_{L1}, \lambda_{L2}, \cdots, \lambda_{Lm})$, $\Lambda_N = diag(\sigma_1^2, \sigma_2^2, \cdots, \sigma_m^2)$, $\Lambda_{N_0} = diag(\lambda_{N_0 1}^2, \lambda_{N_0 2}^2, \cdots, \lambda_{N_0 m}^2)$, $\Lambda_{N_g} = diag(\lambda_{N_g 1}^2, \lambda_{N_g 2}^2, \cdots, \lambda_{N_g m}^2)$. Because $Rank(L) < m$, if $Rank(L) = k$, we will get that $\lambda_{Li} \neq 0 (i \leq k)$ and $\lambda_{Li} = 0 (k < i \leq m)$. According to the equation (8), the minimum eigenvalue is

$$\lambda_{min} = \lambda_m = \lambda_{Lm} + \sigma_m^2 = \sigma_m^2 \tag{9}$$

Hence, we will discuss the item σ_m^2 in detail. Since $N = N_0 + N_g$ and $\sigma_{N_g i}^2 = \sigma^2 (i = 1, 2, \cdots, m)$, where σ^2 is the variance of the Gaussian noise, that

$$\lambda_{min} = \sigma_{N_0 m}^2 + \sigma^2 \tag{10}$$

Thus the perturbation component and the Gaussian noise decide the minimum eigenvalue together. If there is no perturbation component, the minimum eigenvalue will simply equal to the variance of the Gaussian noise that depends on the background noise.

3. **METHODOLOGY.** In this section, the proposed image splicing forgery detection scheme is presented which is illustrated by Fig.1. The subsections are organized as follows: first, an image is segmented into pixel-centered overlapping image blocks. Each block is resampled by the self similarity pixel strategy (SSS) introduced in subsection 3.1. Then, analyze the local minimum eigenvalues of the sample matrix calculated by PCA and present the theory of splicing detection in subsection 3.2. Finally, the proposed algorithm is summarized.

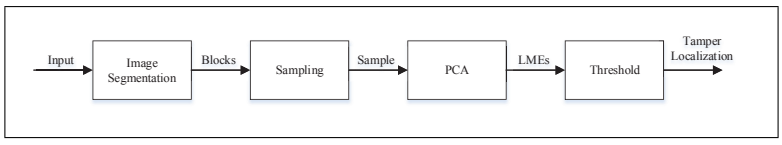

FIGURE 1. Proposed image splicing detection scheme.

3.1. **Self Similarity Pixel Strategy.** For a two-dimensional digital image, each pixel's gray value and spatial location contain all the characteristics of the whole image. As for the local structure characteristic of an image, it is represented by the connected neighbor areas with different gray values. Thus, in order to retain the local structure characteristic of the image better, the self similarity pixel strategy (SSS) is employed to get sufficient samples with a sliding window.

For an image block B with size $L \times L$, set a $K \times K$ sliding window and model the neighbor pixels within the window as a vector which is denoted by $x_i = [x_{1i}\ x_{2i}\ \cdots\ x_{mi}]^T (i = 1, 2, \cdots n)$, $m = K \times K$, as shown in Fig.2, the red window means the first sampling with the window length of $K \times K$, and then moves the window from left to right and top to bottom with one pixel point, just like the yellow window. Therefore, $(L-K+1)^2$ samples can be obtained to constitute a sample matrix $X = [\mathbf{x}_1\ \mathbf{x}_2\ \cdots\ \mathbf{x}_n]$, where $n = (L-K+1)^2$. This sample method is called self similarity pixel strategy (SSS) [20] which permits a reliable similarity measure involving perturbation pixels falling far away from each other.

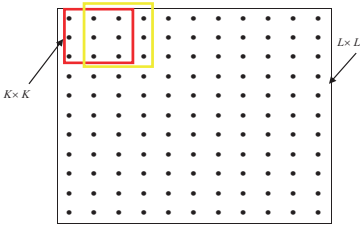

FIGURE 2. Sampling model.

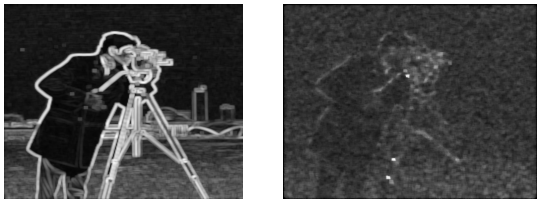

(a) (b)

FIGURE 3. (a)LMEs computed directly; (b)LMEs computed by SSS.

3.2. **Local Minimum Eigenvalue.** Since the image local structure feature can be described by a set of neighbor pixels, an overlapped segmentation scheme is introduced. To compute the minimum eigenvalue at each pixel location (i, j), the block $B_{i,j}$ collected from all surrounding rectangular windows of (i, j) is used for sampling. Further, the SSS is employed to recreate textures and get sufficient samples from the block $B_{i,j}$, which can reduce the effect of small samples and perturbation pixels. All of these minimum eigenvalues are called Local Minimum Eigenvalues (LMEs).

As shown in Fig.3, the edge and texture will been treated as the noise if $B_{i,j}$ is taken directly as the input image of PCA. However, the LMEs mostly depend on the background noise and have a stable distribution after sampling by SSS. Below the LME refers to the local minimum eigenvalue obtained after sampling by SSS if there's no declaration.

Fig.4 is the frequency histogram and the kernel density estimation of the LMEs. It shows that the LMEs concentrate on a small interval. We select the LMEs corresponding to the peak of the kernel density curve as the ME of the image. Fig.5 shows the mean ME of images in TID2008 database [21] changing with the additive noise. From the Fig.5, the ME is sensitive to the noise. What's more, the changing trend of the ME and the noise level are consistent, which gives the basis to distinguish the tampered region from the original image with different background noises.

In order to measure the concentricity of LMEs, the Lorenz curve is drawn, which is shown in Fig.6 and the responding Gini coefficient is computed. In particular, if all data are concentrated in several intervals, Lorenz curve will become concave fold line. For a quantification measure, the Gini coefficient G is obtained by $G = A/(A + B)$. If G is closer to 1, it indicates the distribution is more centralized and vice versa.

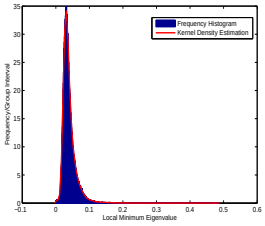

FIGURE 4. Frequency histogram and the kernel estimation of the LMEs

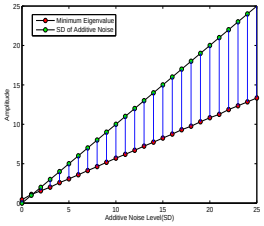

FIGURE 5. The changing trend of the ME and density estimation of the LMEs

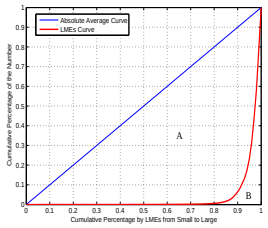

FIGURE 6. Lorenz curve of the cameraman image

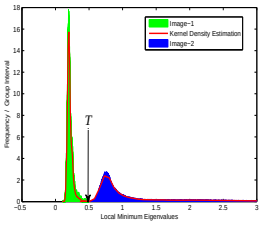

FIGURE 7. Detection threshold

The concentration degree of LMEs is tested by using some of existing image datasets [21–23], and the result is shown in Table 1. As can be seen, the LMEs are highly concentrated in a certain interval and affected little by edges, axis and brightness etc. According to the different intervals that images having different background noise focus on, as shown in Fig.7, we can detect tampered images and localize the tampered region by threshold T at the same time.

TABLE 1. Concentration degree

Dataset	Gini Mean Coefficient	Gini Variance Coefficient	Image Number
BSDS300(test)	0.9158	0.0042	100
BSDS500(test)	0.9206	0.0040	200
Tid2008	0.9293	0.0048	25

3.3. **Algorithm.** The proposed method can be summarized as follows:

- Image segmentation. The block $B_{i,j}$ collected from all surrounding rectangular windows of (i, j) at each pixel location (i, j) with an overlapping segmentation.
- Sample collection. Sample each image block $B_{i,j}$ by using the self similarity pixel strategy(SSS) described in subsection 3.1.
- PCA. For each sample matrix $X_{i,j}$, apply PCA to it and obtain the LME $\lambda_m^{(i,j)}$.
- Thresholding. Set a threshold T to separate the LMEs into two clusters. The threshold T can be obtained by the frequency histogram shown in Fig.7. The detection region can be localized:

$$region(i,j) = \begin{cases} 0\ , & if\ \lambda_m^{(i,j)} < T \\ 1, & else \end{cases} \tag{11}$$

- Post-processing. Use an area threshold to remove small isolated regions.

3.4. **Complexity analysis.** The proposed image splicing detection method mainly contains two phases: the first phase is image overlapping segmentation and the second phase is the application of PCA to each block. For a $N_1 \times N_2$ image, $N_1 \times N_2$ image blocks are obtained by using pixel-centered overlapping segmentation method. Then, PCA is applied to each image block which is sampled by a sliding window with size $K \times K$ to get the minimum eigenvalue and the time complexity of PCA is $O(K^4[(L-K+1)^2+K^2])$. Thus, the total time complexity of our method is $O(N_1N_2K^4[(L-K+1)^2+K^2])$, where $m = K \times K$, $n = (L-K+1)^2$, that is $O(N_1N_2m^2(m+n))$.

4. Experiment results and analysis.

4.1. Image datasets and Evaluation metrics.

4.1.1. *Datasets.* In this paper, the Columbia uncompressed image splicing detection evaluation dataset [24] is employed in our experiments and the compared methods are also conducted on this dataset.

There are total 180 spliced images with almost similar illumination, each of which is stored in the TIFF format and has a resolution ranging from 757×568 pixels to 1152×768 pixels without any post processing. The authentic images are taken with 4 cameras: Canon G3, Nikon D70, Canon 3500 Rebel XT, and Kodak DCS 330. Every 30 spliced images are created for each camera pair, therefore we get total 180 images in the spliced category. Moreover, every spliced image has its own color reference map indicating the original and spliced regions, which can be used for performance evaluation.

Additionally, to further demonstrate the effectiveness of our method, we ourselves compose some spliced images with unnoticeable splicing boundary.

4.1.2. *Evaluation Metrics.* To evaluate the performance of the proposed method, the visual detection results are first displayed and analyzed from the qualitative perspective. Then, several metrics are employed to evaluate the performance in terms of TPR (True Positive Rate), FPR (False Positive Rate) and ACC (Accuracy) quantitatively, which are calculated by

$$TPR = \frac{TP}{TP+FN} \times 100\% \tag{12}$$

$$FPR = \frac{FP}{FP+TN} \times 100\% \tag{13}$$

$$ACC = \frac{TP+TN}{TP+FN+FP+TN} \times 100\% \tag{14}$$

For the full dataset, we employ the Area Under roc Curve (AUC) curve obtained through the receiver operator characteristics (ROC) curve as a measurement in the Columbia dataset.

4.2. Detection Performance.

4.2.1. *Results on single spliced image.* The images used in the experiment are picked randomly from the Columbia dataset [24]. For visual contrast, a tampered image is taken as an example and the detection procedure is show in detail in Fig.8. Fig.8 (a) is the original image suffering from splicing tampering. By refactoring all LMEs obtained through PCA, a LMEs feature image can be get, which is presented in Fig.8 (b). The tampered and original regions are able to be differentiated initially. However the regions are neither clear nor certain. Then a hard threshold or a clustering method can be used to segment the regions. In this paper, the threshold can be obtained through the histogram directly, which is illustrated in Fig.7. The segmented image is shown in Fig.8(c). There is a clear distinction between tampered and original area except for some small

deviations. Finally, an area threshold is applied to remove small isolated regions for connecting the detected regions. The final result is displayed in Fig.8 (d). The detection results demonstrate that the proposed method can find the tampered region and locate the region with reasonable accuracy.

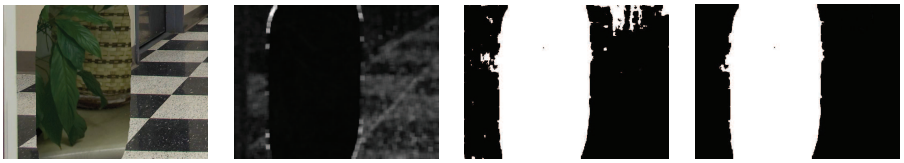

(a) (b) (c) (d)

FIGURE 8. Detection processing analysis.

In order to explain the performance, we compare our method with two region based methods [15, 17]. Four examples of the forged images, together with their detection results by these two methods are shown in Fig.9. It is obvious that our segmentation area is more complete, more continuous and exists less false or missed detection points, which gives a visual representation that our method is much more effective to distinguish tampered regions from those in the original images.

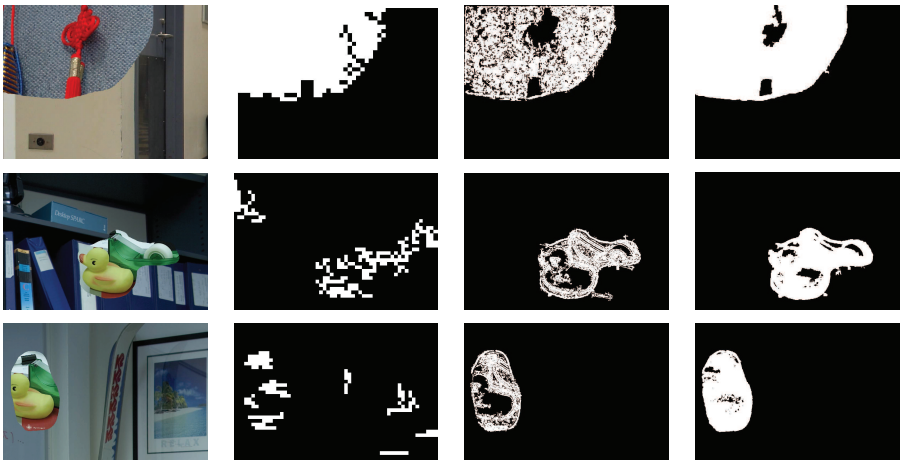

Forged images Mahdian [15] Pan [17] Our method

FIGURE 9. Comparison results.

TABLE 2. Detection accuracy of the four images by three methods

Image	Metrics	Mahdian *et al.* [15]	Pan *et al.*[17]	Proposed method
	TPR	36.28%	89.81%	94.79%
Image 1	FPR	5.55%	3.17%	0.31%
	ACC	62.93%	93.03%	97.45%
	TPR	91.44%	84.45%	99.98%
Image 2	FPR	0.41%	0.59%	2.30%
	ACC	94.79%	93.55%	98.59%
	TPR	32.09%	76.87%	99.34%
Image 3	FPR	5.19%	4.82%	6.67%
	ACC	85.56%	92.48%	94.22%
	TPR	32.98%	83.47%	99.42%
Image 4	FPR	2.69%	0.54%	1.17%
	ACC	90.12%	97.67%	98.90%

Furthermore, we make a numerical experiment to compare the proposed methods with Mahdian *et al.* [15] and Pan *et al.*[17]. For each detection image, we compared it to the

respective color reference map at the pixel level and calculated the TPR, FPR, and ACC metrics as shown in Table 2. The quantitative results show that the proposed method has a higher TPR and ACC than the other two methods, which well suggests the availability of our method.

As a more realistic test, three images are manipulated by Photoshop. As shown in Fig.10, these forgeries have realistic appearance after being manipulated and post-processed. The proposed method can achieve a higher detection precision under the same condition by contrast. What's more, the detection regions by proposed method are more integrated and tampered edges are much more continual.

Original 1 Original 2 Forged image Pan [17] Our method

FIGURE 10. A realistic test.

4.2.2. *Results on full dataset.* The experiment above has primarily indicated that the proposed method tends to have a better result on the single image. Next, we will illustrate its effect on the full Columbia dataset by giving the ROC curves of these three methods (both the false position rate and the true position rate are the mean of this image set) in Fig.11 (a). It shows that the proposed method can achieve a higher TPR at the same FPR, which is obvious that the proposed method and the method in [17] have a better performance. Hence, to further demonstrate the detection effect of the proposed method, the AUCs of each image in the Columbia dataset obtained by these two detection methods are compared with by a scatter chart in Fig.11 (b). It can be seen that our method's performances are much better than the Xunyu Pan's in most cases.

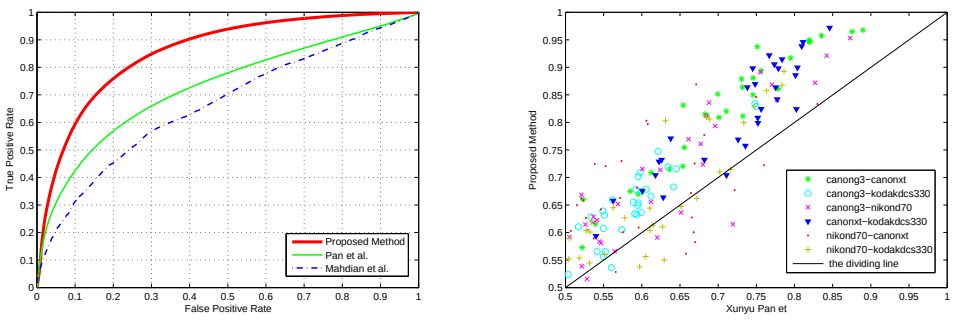

(a) (b)

FIGURE 11. (a) Mean ROC of Columbia dataset; (b) AUC comparison scatter.

In addition, Table 3 gives the statistics of AUCs about all the images classified by the cameras in this image dataset. These are the indicators that the proposed method can

TABLE 3. Performance quantitative evaluation

Cameras	Numbers	Mahdian *et al.* [15] E(AUC)	Pan *et al.* [17] E(AUC)	Proposed Method E(AUC)
canong3canonxt	30	0.6363	0.7094	0.8219
canong3kodakdcs330	30	0.6481	0.5849	0.6642
canong3nikond70	30	0.6440	0.6366	0.7050
canonxtkodakdcs330	30	0.6439	0.7204	0.8088
nikond70canonxt	30	0.6293	0.6005	0.6839
nikond70kodakdcs330	30	0.6468	0.6207	0.6318
Total	180	0.6414	0.6454	0.7193

apply to detect splicing images with regions from other images and achieve much higher detection accuracy than the method in [15, 17], subject to data and statistics.

5. **Conclusions.** In this paper, a novel effective image splicing forgery detection method is proposed based on the concentricity of local minimum eigenvalues calculated by using PCA. This method is suitable for any input splicing forgery images with inconsistent irrelevant components. It can localize the tampered region on the pixel level. What's more, the minimum eigenvalue exists as a property that only relates to image itself. It can be available by direct calculation without the estimation procedure, which eliminates the estimation errors affected by estimation methods and further increases the detection precision.

The paper validates the concentricity of the minimum eigenvalues through Gini coefficient with existing picture galleries. Then apply our method to detect splicing images in image database and manipulated by Photoshop. All experimental results show that the proposed method can not only achieve high detection accuracy, but also yield complete detection regions with continual edges as well.

Acknowledgements. This work was supported by Shenzhen Engineering Laboratory of Broadband Wireless Network Security, and the Science and Technology Development Fund of Macao SARFDCT056/2012/A2 and UM Multi-year Research Grant MYRG144(Y1-L2)-FST11-ZLM.

REFERENCES

[1] Z. Qu, G. Qiu, and J. Huang, Detect digital image splicing with visual cues, *Lecture Notes in Computer Science*, vol. 5806, pp. 247–261, 2009.

[2] G. Gu, J. Zhu, Z. Liu, and Y. Zhao, Visual saliency detection based object recognition, *Journal of Information Hiding and Multimedia Signal Processing, vol. 6, no. 6*, pp. 1250–1263, Nov. 2015.

[3] Z. Fang, S. Wang, and X. Zhang, Image splicing detection using color edge inconsistency, *IEEE International Conference on Multimedia Information Networking and Security (MINES)*, pp. 923–926, 2010.

[4] H. Farid, Detecting digital forgeries using bispectral analysis, *MIT AI Memo AIM-1657, MIT*, 1999.

[5] D. Fu, Y. Q. Shi, and W. Su, *Detection of Image Splicing Based on Hilbert-Huang Transform and Moments of Characteristic Functions with Wavelet Decomposition.* Springer Berlin Heidelberg, 2006.

[6] Y. Sutcu, B. Coskun, H. T. Sencar, and N. Memon, Tamper detection based on regularity of wavelet transform coefficients, *Proceedings ICIP International Conference on Image Processing*, pp. 397–400, 2007.

[7] T.-T. Ng, Camera response function signature for digital forensics-part ii: signature extraction, *IEEE International Workshop on Information Forensics and Security*, pp. 161–165, 2009.

[8] X. Zhao, J. Li, S. Li, and S. Wang, Detecting digital image splicing in chroma spaces, *Proceedings of the 9th international conference on Digital watermarking*, 2010.

[9] M. Z, J. HA, M. N. R, and A. S, Improving rlrn image splicing detection with the use of pca and kernel pca, *Scientific World Journal*, vol. 2014, pp. 1–16, 2014.

[10] M. S. Lai, H. C. Huang, and S. C. Chu, Image texture segmentation with ant colony systems., *International Conference on Innovative Computing Information and Control, ICICIC*, pp. 652–656, 2006.

[11] T. Xiong and Y. Huang, Robust gaussian mixture modelling based on spatially constraints for image segmentation, *Journal of Information Hiding and Multimedia Signal Processing, vol. 6, no. 5*, pp. 857–868, Sep.2015.

[12] J. Lukáš, J. Fridrich, and M. Goljan, Detecting digital image forgeries using sensor pattern noise, *Electronic Imaging 2006*, pp. 60720Y–60720Y, 2006.

[13] A. C. Popescu and H. Farid, Exposing digital forgeries in color filter array interpolated images, *IEEE Transactions on Signal Processing*, vol. 53, no. 10, pp. 3948–3959, 2005.

[14] M. K. Johnson and H. Farid, Exposing digital forgeries in complex lighting environments, *IEEE Transactions on Information Forensics and Security*, vol. 2, no. 3, pp. 450–461, 2007.

[15] B. Mahdian and S. Saic, Using noise inconsistencies for blind image forensics, *Image and Vision Computing*, vol. 27, no. 10, pp. 1497–1503, 2009.

[16] X. Pan, X. Zhang, and S. Lyu, Exposing image forgery with blind noise estimation, *Proceedings of the thirteenth ACM multimedia workshop on Multimedia and security*, pp. 15–20, 2011.

[17] X. Pan, X. Zhang, and S. Lyu, Exposing image splicing with inconsistent local noise variances, *IEEE International Conference on Computational Photography (ICCP)*, pp. 1–10, 2012.

[18] H. Abdi and L. J. Williams, Principal component analysis, *Wiley Interdisciplinary Reviews: Computational Statistics*, vol. 2, no. 4, pp. 433–459, 2010.

[19] E. J. Candès, X. Li, Y. Ma, and J. Wright, Robust principal component analysis?, *Journal of the ACM (JACM)*, vol. 58, no. 3, p. 11, 2011.

[20] K. J. Peter, D. K. S. Kannan, D. S. Arumugan, and G. Nagarajan, Two-stage image denoising by principal component analysis with self similarity pixel strategy, *International Journal of Computer Science and Network Security*, vol. 11, no. 5, pp. 296–301, 2011.

[21] N. Ponomarenko, V. Lukin, A. Zelensky, K. Egiazarian, M. Carli, and F. Battisti, Tid2008-a database for evaluation of full-reference visual quality assessment metrics, *Advances of Modern Radioelectronics*, vol. 10, no. 4, pp. 30–45, 2009.

[22] D. Martin, C. Fowlkes, D. Tal, and J. Malik, A database of human segmented natural images and its application to evaluating segmentation algorithms and measuring ecological statistics, *IEEE International Conference on Computer Vision*, vol. 2, pp. 416–423, 2001.

[23] P. Arbelaez, M. Maire, C. Fowlkes, and J. Malik, Contour detection and hierarchical image segmentation, *IEEE Transactions on Pattern Analysis and Machine Intelligence*, vol. 33, no. 5, pp. 898–916, 2011.

[24] Y.-F. Hsu and S.-F. Chang, Detecting image splicing using geometry invariants and camera characteristics consistency, *IEEE International Conference on Multimedia and Expo*, pp. 549–552, 2006.